

Time-resolved single-photon detection module based on silicon photomultiplier: A novel building block for time-correlated measurement systems

E. Martinenghi, L. Di Sieno, D. Contini, M. Sanzaro, A. Pifferi, and A. Dalla Mora

Citation: [Review of Scientific Instruments](#) **87**, 073101 (2016); doi: 10.1063/1.4954968

View online: <http://dx.doi.org/10.1063/1.4954968>

View Table of Contents: <http://scitation.aip.org/content/aip/journal/rsi/87/7?ver=pdfcov>

Published by the [AIP Publishing](#)

Articles you may be interested in

[Multiple wavelength time-of-flight sensor based on time-correlated single-photon counting](#)

Rev. Sci. Instrum. **76**, 083112 (2005); 10.1063/1.2001672

[Full correlation from picoseconds to seconds by time-resolved and time-correlated single photon detection](#)

Rev. Sci. Instrum. **76**, 083104 (2005); 10.1063/1.1946088

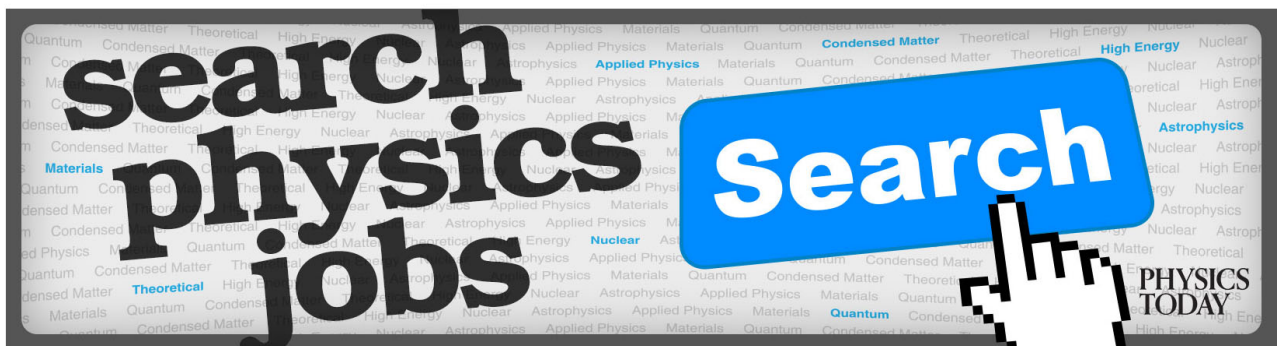
[Time-autocorrelated two-photon counting technique for time-resolved fluorescence measurements](#)

Rev. Sci. Instrum. **70**, 41 (1999); 10.1063/1.1149540

[Fast photomultiplier tube gating system for photon counting applications](#)

Rev. Sci. Instrum. **69**, 4068 (1998); 10.1063/1.1149252

[APL Photonics](#)



Time-resolved single-photon detection module based on silicon photomultiplier: A novel building block for time-correlated measurement systems

E. Martinenghi,^{1,a)} L. Di Sieno,¹ D. Contini,¹ M. Sanzaro,² A. Pifferi,^{1,3} and A. Dalla Mora¹

¹*Dipartimento di Fisica, Politecnico di Milano, Piazza Leonardo da Vinci 32, 20133 Milano, Italy*

²*Dipartimento di Elettronica, Informazione e Bioingegneria, Politecnico di Milano, Piazza Leonardo da Vinci 32, 20133 Milano, Italy*

³*Istituto di Fotonica e Nanotecnologie, Consiglio Nazionale delle Ricerche, Piazza Leonardo da Vinci 32, 20133 Milano, Italy*

(Received 29 January 2016; accepted 16 June 2016; published online 5 July 2016)

We present the design and preliminary characterization of the first detection module based on Silicon Photomultiplier (SiPM) tailored for single-photon timing applications. The aim of this work is to demonstrate, thanks to the design of a suitable module, the possibility to easily exploit SiPM in many applications as an interesting detector featuring large active area, similarly to photomultiplier tubes, but keeping the advantages of solid state detectors (high quantum efficiency, low cost, compactness, robustness, low bias voltage, and insensitiveness to magnetic field). The module integrates a cooled SiPM with a total photosensitive area of 1 mm² together with the suitable avalanche signal read-out circuit, the signal conditioning, the biasing electronics, and a Peltier cooler driver for thermal stabilization. It is able to extract the single-photon timing information with resolution better than 100 ps full-width at half maximum. We verified the effective stabilization in response to external thermal perturbations, thus proving the complete insensitivity of the module to environment temperature variations, which represents a fundamental parameter to profitably use the instrument for real-field applications. We also characterized the single-photon timing resolution, the background noise due to both primary dark count generation and afterpulsing, the single-photon detection efficiency, and the instrument response function shape. The proposed module can become a reliable and cost-effective building block for time-correlated single-photon counting instruments in applications requiring high collection capability of isotropic light and detection efficiency (e.g., fluorescence decay measurements or time-domain diffuse optics systems). © 2016 Author(s). All article content, except where otherwise noted, is licensed under a Creative Commons Attribution (CC BY) license (<http://creativecommons.org/licenses/by/4.0/>). [<http://dx.doi.org/10.1063/1.4954968>]

I. INTRODUCTION

A wide number of Time-Correlated Single-Photon Counting (TCSPC)¹ applications (e.g., fluorescence decay measurements and time-domain diffuse optics systems^{2–12}) need large-area detectors, which are able to acquire very faint isotropically distributed light signals down to the single-photon level with high timing resolution (few hundreds picoseconds). The unceasing trend towards compact and reliable optical measurement systems for on-the-field applications^{13,14} requires a dedicated development of suitable, cost-effective, and easy-to-use building blocks. In the specific case of faint isotropic light detection in the time-domain, the common choice is the use of photocathode-based detectors like Photomultiplier Tubes (PMTs). Unfortunately, a widespread use of PMT-based systems outside laboratories is often impaired by some related disadvantages. Indeed, PMTs typically feature low quantum efficiency in the near-infrared range and they are quite expensive, bulky, fragile, and sensitive to magnetic fields. In particular, the exposure to intense light can have a permanent detrimental effect on the photocathode performances.

Over the past few years, the need for low cost, rugged, and compact systems had brought to the wide spread of solid-state single-photon detectors such as Single-Photon Avalanche Diodes (SPADs).¹⁵ SPADs hold the potential to knock-down the system cost and complexity and are insensitive to both intense light exposure and high magnetic fields. Indeed, SPADs do not need complex front-end circuitry;¹⁵ therefore, they can be easily integrated into a single chip together with the detector, thus allowing arrangements that are truly miniaturized (in principle, down the dimension of the single chip), in particular, when also the TCSPC circuitry is embedded.^{16–18} In addition, they have been recently considered in diffuse optics because they allow the use of small source-detector separations, thanks to the possibility of exploiting an efficient mechanism of time-gating to reject scarcely diffused photons that otherwise will saturate the detector.^{19,20} Unfortunately, the use of SPADs is demoted due to their small detection area (tens or hundreds μm diameter) which limits the signal harvesting, since signal from spread isotropic light emitters cannot be efficiently focused into a small spot without significant losses.

To overcome this limitation, a possible solution is to increase the detector active area, but this will produce a sensible worsening in performances like Single-Photon Time-Resolution (SPTR) and Dark Count Rate (DCR). The SPTR

^{a)}Electronic mail: edoardo.martinenghi@polimi.it



reduction is due to the increased dispersion of the avalanche build-up,²¹ while the DCR increases with the active area, where the dominant contribution can be ascribed to the higher effect of the afterpulsing²² due to the augmented avalanche current flow within large-area devices.²³

An alternative solution for increasing the detection area of solid-state devices is to parallelize multiple SPADs with high density. Such a solution permits to maximize the ratio between effective active area and the dead region between devices, thus realizing the so-called Silicon Photomultiplier (SiPM)^{24,25} which is basically an array of microcells constituted by a small diameter SPAD (typically tens μm) together with an integrated quenching resistor for the avalanche passive quenching and self-reset. All microcells are connected together to create a two terminals detector, with one global anode and one global cathode. This kind of detector holds the advantages of both solid-state detectors and photocathode-based ones, featuring: high quantum efficiency in the near-infrared range, low cost and complexity, compactness, robustness, low bias voltage, insensitiveness to magnetic field, and large active areas.

Until very recently, the use of this kind of detectors in single-photon applications has been relegated by their poor SPTR and high DCR. However in the last few years, SiPMs have experienced a huge technological improvement, thanks to their wide application in high-energy physics²⁶ and Positron Emission Tomography (PET) systems,²⁷ thus leading to impressive performances with SPTR lower than 60 ps.²⁸ This enhancement has paved the way for the successful demonstration of time-resolved SiPM for fluorescence applications²⁹ and the design of SiPMs-based diffuse optics systems,^{30–32} thus in principle, drastically reducing the system complexity and cost. However, these potentialities are still to be fully achieved since, up to now, SiPM was operated for single-photon timing using custom designed front-end electronic circuitry and bulky and expensive laboratory instruments (e.g., radio frequency (RF) amplifiers, bench power supply generators), thus requiring strong skills for the detector operation and demoting a wide spread use of this technology. Similarly to what happened for SPADs, there is now the need to develop suitable, stand-alone, and plug-and-play single-photon counting modules, which must be easy to use for a broad scientific community, while keeping the high performances of the previous implementations (i.e., SPTR of about 100 ps, clean instrument response function (IRF) without bumps or non-linearity, and well-detectable output signal level). To the best of our knowledge, a certain number of SiPM-based modules is known in the literature (i.e., Multi-Pixel Photon Counter (MPPC) module by Hamamatsu Photonics, Lynx SiPM module by Excelitas Technologies, MiniSM module by Sensl, and others) but none of them demonstrated the possibility to efficiently extract the single-photon timing information from the detector, being mainly tailored for photon-number resolving applications.

The aim of this paper is to address this need by demonstrating the possibility to easily exploit SiPM advantages in many applications, thanks to the design, fabrication, and general-purpose characterization of a high performance SiPM-based single-photon timing module. This instrument repre-

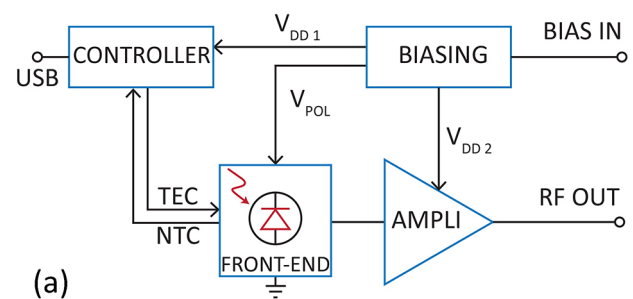
sents a fundamental building block for SiPM based systems, opening the possibility of easy and low-cost parallelization, with reliable and stable performances.

Our module is completely stand-alone and it is able to extract the arrival times of the photons on the detector (1 mm² area SiPM produced by Excelitas, Canada), preserving the intrinsic SPTR, hence obtaining an overall resolution of about 100 ps. In addition, the stabilization of the detector temperature makes the performances to be constant over time even in the presence of external temperature perturbations.

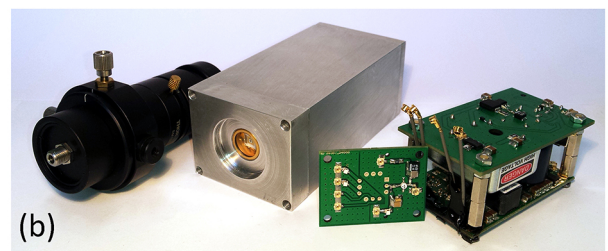
II. MODULE DESCRIPTION

Figure 1(a) shows the block scheme of the module: the core is the “front-end” part that embeds the SiPM (C30742-11-050-T1, Excelitas Technologies, Canada) together with a passive high-pass filter read-out circuitry (the vertical board in Figure 1(b)). When a single-photon reaches the detector active area and triggers the avalanche process, the current is converted into a voltage pulse by the passive network. This pulse enters into a single-stage amplifier based on a Monolithic Microwave Integrated Circuit (MMIC) that provides the amplified signal to the timing output of the module through a SubMiniature version A (SMA) coaxial connector. The RF layout is crucial to preserve the detector timing resolution by avoiding the degradation of the fast (~ 1 ns) and faint (~ 1 mV) avalanche pulse.

The SiPM is packaged together with a Thermo-Electric Cooler (TEC) element and a Negative Temperature Coefficient (NTC) resistor. A miniaturized commercially available TEC controller board (Meerstetter Engineering GmbH, Switzerland) is embedded into the module (the horizontal bottom board in Figure 1(b)) to precisely monitor the detector



(a)



(b)

FIG. 1. Block schematic of the system (a): the CONTROLLER, programmable by an USB connection, drives the thermoelectric cooler (TEC) and reads the device temperature through a negative temperature coefficient NTC resistor; the voltage amplitude of the avalanche signal is raised by a RF amplifier (AMPLI) and provided to the analog output (RF OUT). The BIASING network provides all the supply voltages from a unique 15 V bias input (BIAS IN). In the bottom part (b) shows a picture of the module (center), with a possible optical system for fiber coupling (on the left) and the three designed electronic boards hosted in the module (on the right).

temperature (with 0.001 °C resolution) and to stabilize it. This temperature can be selected in the range between -10 °C and 50 °C by a Universal Serial Bus (USB) connection to a personal computer with dedicated software, commercially available with the controller. However, the presence of a personal computer is only needed to change the temperature setting, since the TEC controller memorizes the last parameters used. The “biasing” board (horizontal top board in Figure 1(b)) is a custom printed circuit board designed to provide all the necessary supply voltages: (i) the TEC controller power supply $V_{DD1} = 12\text{ V}$; (ii) the detector biasing high voltage, V_{POL} , that can be selected between 0 and 200 V; and (iii) the Radio Frequency (RF) amplifier operation voltage $V_{DD2} = 10\text{ V}$. This board requires a supply voltage of 15 V through a power jack connector using an external plug in AC power adapter. The total power consumption of the module mainly depends on the TEC controller settings, reaching the maximum value of about 6 W when the controller is delivering the maximum current to the Peltier element.

Figure 1(b) shows a picture of different parts of the module: (i) a general purpose focusing optics. It is composed of a standard M1 optical mounting tube (on the left) which holds the optical fiber (multimode step index fiber with 1 mm core, $NA = 0.39$, 2 m long, M35L02 Thorlabs GmbH, Germany). After the holder for the fiber, an XY stage (LM1XY/M, Thorlabs GmbH, Germany) is mounted so as to properly focus light on the detector and then two achromatic doublet lenses (AC254-030-B from Thorlabs GmbH, diameter 25.4 mm and focal lens 30 mm) are present to provide a $1\times$ magnification. Just before the detector, a shutter (SM1SH1, Thorlabs GmbH, Germany) is mounted, which is able to keep the detector in the dark when needed to characterize the dark count rate; (ii) the complete module hosted in a metal external case to shield the internal electronic boards from possible environment electromagnetic interferences (center); and (iii) the three electronic boards hosted in the module without the external case (right side).

The external case features extremely compact dimensions ($5\text{ cm} \times 4\text{ cm} \times 100\text{ cm}$).

III. MODULE CHARACTERIZATION

A. Thermal stability

Thermal perturbations are often among the most threatening issues for measurement systems. Considering a solid state detector like a SiPM, a number of parameters depends on the detector temperature, for instance the DCR, the breakdown voltage, and the values of integrated resistors, thus also affecting related performances such as the SPTR and temporal response shape. Even if the instrumentation temperature can be easily controlled when employed inside a laboratory, in a real-field application, it becomes difficult. The module here reported is intended for on-field applications such as clinical diagnosis, where it is possible to have room temperature fluctuations, or food quality assessment during harvesting¹³ where thermal perturbations are very common being in plantations. For this reason, the effective temperature stabilization is a crucial feature; indeed, we proved the thermal stability of the system by giving a sequence of a controlled heat perturba-

tion followed by a cooling one. Two identical modules were placed together side by side, with a thermal conductive paste in between to minimize the thermal resistance, thus imposing the same temperature of the two external metal cases. This temperature was monitored by a thermocouple sensor inserted between the two modules. In order to compare the different effects of the perturbation, one module was fully stabilized by enabling the TEC controller, whereas the other one was kept with the thermal stabilization powered off.

Before starting the measurement, the modules were off at the temperature of 21.1 °C . Then, both modules were simultaneously powered on. After a normal (without perturbation) warm-up of 15 min, the case temperature reached 24 °C . We then produced the first perturbation by heating both cases with an air flux at the temperature of 130 °C , almost uniformly distributed over the system for 20 s, with the consequence of heating the cases at 33 °C . After the heating, the system was left free to cool down for 200 s, reaching 26.6 °C . After that, the cold perturbation was produced with a cooling flux at -50 °C for 200 s, which lowered the cases temperature down to 4.7 °C . Finally, the system was monitored without other perturbations for 14 min and in the end the system reached a temperature of 25.6 °C .

To quantify the perturbation induced on the detectors, we analyzed and considered as the most relevant parameter the variation of the DCR: in fact, in this temperature range (where the afterpulsing is almost negligible as it will be shown in Sec. III C), the spontaneous generation of electron-hole pairs depends monotonically (almost exponentially) on the device temperature.¹⁵ To ensure that only the DCR was considered, we closed the optical shutter on the detector, to avoid any photon reaching the SiPM active area.

The two curves shown in Figure 2 represent the DCR variations recorded by the two modules over time: the lower

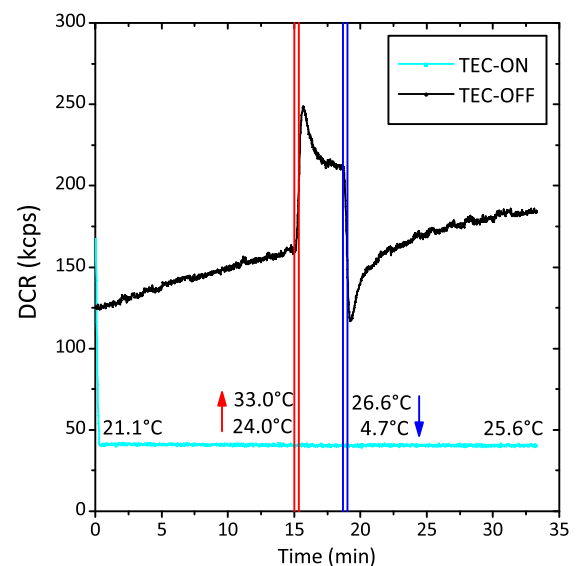


FIG. 2. Modules DCR response to thermal perturbations when the TEC controller is, respectively, powered on (cyan bottom horizontal line) and off (black top line). The external metallic case temperature is reported and it is the same for both modules, being them thermally connected. It is clear the effect of the stabilization network, which makes the module completely insensitive to perturbations and significantly speeds-up the initial warm-up.

cyan one is for the module with the active TEC controller stage, whereas the upper black curve refers to the module with the controller kept off. A fast warm up during the first minute can be noticed for the stabilized module since the measurement started when both modules were just powered on. As it is evident, the stabilized module is completely insensitive to both positive and negative temperature perturbations produced on its case, thus proving the effectiveness of the active thermal stabilization stage. On the contrary, the other module suffers from a slowly varying baseline, related to the system warm up, which does not settle to a fixed point for all the measurement duration. Additionally, superposed to that slow variation, strong DCR variations (about 70%) can be appreciated in response to the thermal stimuli.

B. Single photon timing resolution and dark count rate

To perform a broadband (500–1100 nm) single-photon timing performance characterization, we used the same setup reported in Ref. 33, where a supercontinuum laser source (NKT Photonics, Denmark) provides a total output power of about 5 W over a large spectrum, spreading from 450 nm to 1750 nm. The white light beam is dispersed by a prism and then coupled into a 50 μm core optical fiber acting as a spatial filter, resulting in a spectral bandwidth of about 10 nm. Spectral scanning is achieved through automated prism rotation. A Neutral Density (ND) attenuator is used to adjust the light power delivered down to the single-photon level. As reported in Ref. 28, the laser provides optical pulses with 10 ps width, well below the SiPM SPTR, thus allowing us to neglect its jitter contribution with respect to the SiPM one.

The histogram of the arrival times of detected photons is reconstructed using a TCSPC board (SPC130, Becker & Hickl GmbH, Germany) hosted into a personal computer. The module output provides the “stop” pulse to the timing board, whereas the “start” signal is given by the laser synchronism, at a repetition frequency of 40 MHz. Even if the module is able to achieve a maximum count rate of about 80 Mcps, which we measured by the means of an electronic counter (53131A, Agilent Technologies, US), we always kept the total photons detection rate below the few percent of the laser repetition rate in order to limit the pile-up effect.¹ Such a choice allows us to get the precise reconstruction of the detector single photon Instrument Response Function (IRF) without introducing any distortion due to the TCSPC measurement.

Figure 3 displays the dependence of both the DCR (left y-axis) and the SPTR (right y-axis), evaluated as the Full-Width at Half Maximum (FWHM) of the acquired IRF curve, over the device excess bias voltage (V_{EX}) calculated as the difference between the polarization voltage (V_{POL}) and the detector breakdown (V_{BD}) at the temperature of 25 °C ($V_{\text{BD}} = 95.6$ V). The primary DCR is usually given by both temperature-assisted processes (i.e., thermal generation of free carriers within the depleted region by Shockley–Read–Hall mechanism) and field-assisted processes (i.e., direct band-to-band and trap-assisted tunneling).³⁴ It is worth noting that both

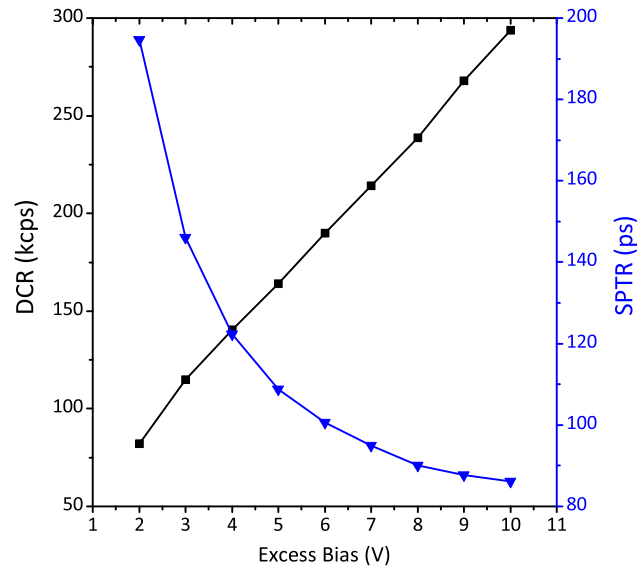


FIG. 3. Dark Count Rate (DCR, left axis) and Single-Photon Timing Resolution (SPTR, right axis) as a function of the excess bias voltage. Increasing the detector polarization will be reflected on one hand into an increase of DCR, but on the other hand into an improvement of the SPTR.

contributions can increase with V_{EX} : the former is indirectly correlated to the electric field because of the higher avalanche triggering probability at high voltages, whereas the latter is directly assisted by the intensity of the electric field. For these reasons, the DCR increases with the excess bias voltage as reported in Figure 3. It is worth noting that the after-pulsing was not subtracted; therefore, this curve is the sum of both primary DCR generation and trap-assisted process. However, our purpose here is not to characterize the detector itself by separating different noise contributions but to characterize the global module performance. The graph reported in Figure 3 helps in finding the best compromise between noise and timing resolution. Considering the SPTR, a high electric field within the junction will speed-up the triggering of the avalanche process, thus reducing the detector jitter.

From this characterization, we selected a reference polarization value for the following measurements, by choosing a V_{EX} of 6 V. At this level, the SPTR is around 100 ps and starts to decrease much slower with the bias, whereas the DCR is still below 200 kcps. Even if this value can look quite high when compared to DCR of photocathode based detectors, in many TCSPC applications, it can be easily tolerated since the signal-to-noise ratio (SNR) of the measurement is not limited by the mean value of the noise. Indeed it can be easily measured and subtracted being uncorrelated to the signal. The SNR limit is instead represented by the standard deviation of its Poissonian distribution, therefore varying as the square root of the overall noise counts. It is worth nothing that while the DCR is essentially an intrinsic property of the SiPM, almost not dependent on the front-end circuitry, the SPTR is strongly dependent on the electronic design. Therefore, a 100 ps resolution for a compact and stand-alone system is a remarkable result, being comparable to the best results previously published in the literature for a single detector with bulky ancillary electronics.^{28,35–37}

C. Noise floor

We also characterized the noise contribution of the SiPM at different photon detection rates, thus highlighting not only the effect of the primary dark carrier generation processes but also the afterpulsing, which is sometimes the dominant contribution to background noise.

Figure 4 reports the measured noise floor of the detector over the device temperature at different photon counting rates, from 0 (only noise) photons per second (pps) up to 1 Mpps. Due to the variation of the breakdown voltage with temperature ($\Delta V_{BD} = 90 \text{ mV}/^\circ\text{C}$), the excess bias voltage has been kept constant (i.e., 6 V) by adapting the detector bias V_{POL} . To evaluate the noise floor at different counting rates, we acquired multiple IRFs by increasing for each measurement the incident laser power to the target photons count rate. For each acquisition, we calculated the background noise by considering the noise floor of TCSPC acquisition. Since the TCSPC board dead time (i.e., hold off time $T_H = 125 \text{ ns}$) can cause the loss of a number of photon counts, we compensated the measured count rate (DCR_M) to obtain the real value (DCR_R) as reported in Ref. 38,

$$DCR_R = DCR_M \times \frac{1}{(1 - DCR_M \times T_H)}. \quad (1)$$

In Figure 4, the DCR tends to reduce on the left side of the graph because the thermal generation decreases by lowering the detector temperature. However, under high photon fluxes, the noise floor at lower temperature is strongly dependent on the photon counting rate since the effect of afterpulsing becomes dominant; the reason of this behavior is that the release time constant of trapped charges increases by decreasing temperature,²² thus giving a background noise mainly dependent on the photon counting rate. Conversely, at higher temperatures, the trapped carriers release rate gets higher, as well as the thermal generation of dark carriers.³⁴ In this way, the afterpulsing contribution becomes negligible with respect to the spontaneous generation of free carriers, thus

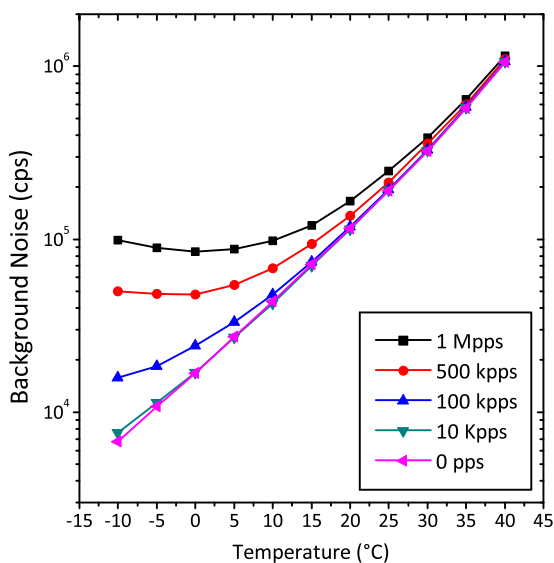


FIG. 4. Measured DCR as a function of the detector temperature at different photon counting rates, from no photon signal (0 pps) up to 1 Mpps.

the background noise becomes almost independent from the photon counting rate. The highest photon counting rate that we measured is 1 Mpps, which can be considered in the order of magnitude of the upper limit for a TCSPC system at tens of MHz of laser repetition rate, as already stated in Section III B. This measurement allows one to quantify the increase of background noise during real operative conditions, thus giving indications to set the proper detector temperature depending on the background noise that can be tolerated in a specific application. For example, the use of low temperatures like -10°C is suggested for applications where photon fluxes are below few hundreds kcps, thus keeping the background noise below few tens of kcps, while for MHz photon arrival rates, the use of a temperature close to 0°C is preferable to minimize the noise by keeping it below 100 kcps.

D. Photon detection efficiency

The Photon Detection Efficiency (PDE) is the probability of registering a count when a photon reaches the detector area. PDE is essentially related to the detector structure and bias, and it is almost independent of the electronic circuit. However, we measured this parameter since unimpeachable electronic design or sensitivity to electromagnetic disturbances can easily produce a loss of counts, thus resulting with a reduction of the effective PDE. Indeed, the faint avalanche pulses produced across the device ($\sim 1 \text{ mV}$) can be overwhelmed by noise due to electromagnetic disturbances.³⁹

The measurement principle adopted for testing the PDE of the SiPM module is a direct comparison with a calibrated photodiode. In particular, to measure the PDE over a wide spectral region, we employed a custom optical setup (the same reported in Ref. 40) composed by: (i) a broadband arc lamp; (ii) optical neutral density filters for attenuating the light down to the single photon level; (iii) a monochromator that can operate in the visible and near-infrared ranges and allows the selection of the wavelength of interest with a spectral resolution of about 10 nm; and (iv) an integrating sphere for guaranteeing a uniform photon flux over both the SiPM and reference detector. The light from the lamp is focused into a slit where the filter wheel is housed. The filtered lamp radiation beam passes through the monochromator and then enters the integrating sphere. Such sphere is provided with three apertures: the first one is connected to the monochromator, the second one uniformly illuminates the detector active area, and the third one is needed for constantly measuring the light power thanks to the calibrated photodiode. The outlined setup was kept in a light-isolated environment.

The detection efficiency has been calculated as the average frequency of net photon detections (i.e., with DCR and afterpulsing subtracted), CR , divided by the average frequency of incoming photons, PR . For each wavelength, λ , PR is given by $\lambda kP/(hc)$, where P is the calibrated photodiode power reading, hc/λ is the energy of the photon, and k is a correction factor which takes into account the active area mismatch between the SiPM detector and the calibrated photodiode. Measurements are simultaneously carried out on both detectors, in order to avoid errors due to fluctuations and drift of the lamp intensity. The SiPM dark count rate was first measured and then

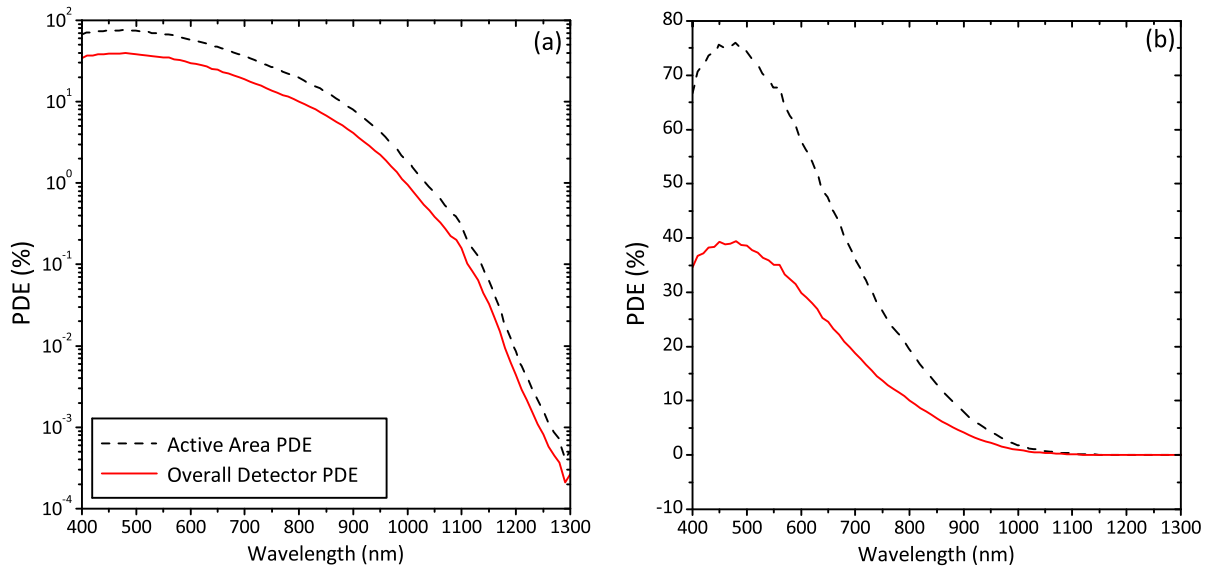


FIG. 5. Measured Photon Detection Efficiency (PDE) at 6 V of excess bias voltage and 25 °C temperature in both logarithmic (a) and linear (b) scales: the bottom solid line is the overall detector efficiency, while the top dashed line is the average efficiency of the active area, which has been obtained rescaling the measured efficiency by the detector fill factor (51%).

subtracted from the count rate when it was exposed to the photon flux, which has been attenuated in order to have a net count rate comparable to the detector DCR (~ 200 kHz), thus minimizing the effect of the afterpulsing and dead time corrections.

In Figure 5, the red bottom line is the PDE measured at 25 °C in the wavelength region between 400 and 1300 nm, with steps of about 10 nm. As explained in Section III B, the detector is biased 6 V above breakdown. At 500 nm, this SiPM features a PDE $> 30\%$ (a spectral region that is particularly interesting for many fluorescence applications), whereas at 800 nm, the PDE is about 10% and it is still about 1% at 1000 nm. For $\lambda > 1100$ nm (i.e., the silicon cut-off wavelength), the slope of the PDE spectrum drastically changes.

The slope of the PDE decay beyond the cutoff is in line with other results previously reported for silicon SPADs.⁴¹ This result is remarkably different with respect to data reported for the data sheet of the SiPM,⁴² where the cut-off wavelength is reported around 800 nm, which is not expected for a silicon detector.

The black dashed line in Figure 5 instead is the efficiency of each elementary cell of the SiPM, which is obtained rescaling the measured efficiency by the detector fill factor (51%), showing a remarkable peak value of 76% at 480 nm. Such values are in agreement with the PDE reported for single thick-junction silicon SPADs in the past⁴³ and set an ideal line on the PDE physical limit that can be achieved by increasing the SiPM fill factor.

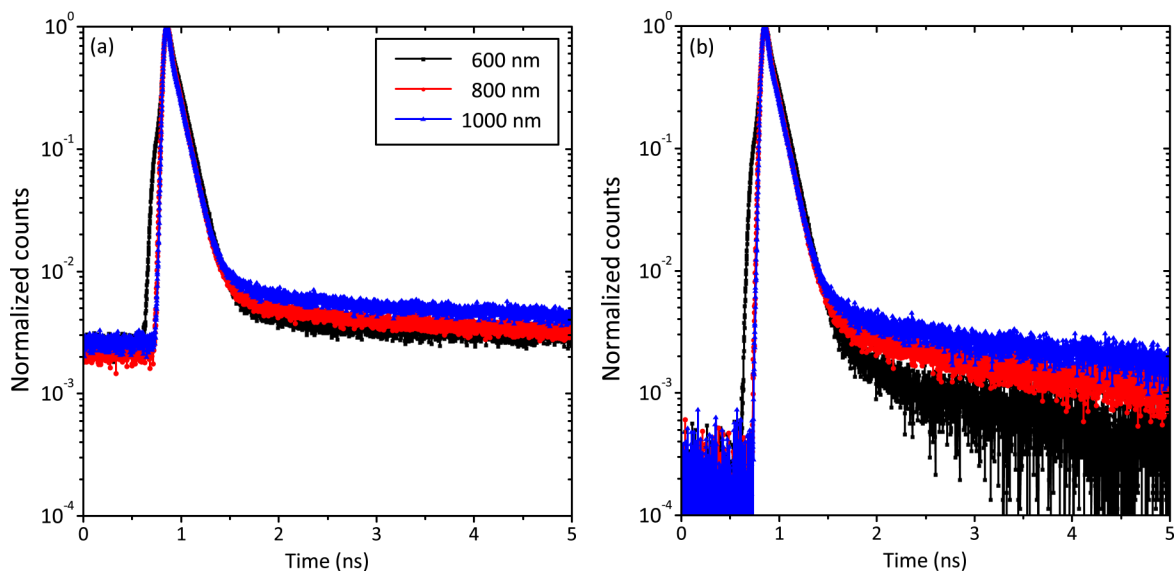


FIG. 6. Instrument Response Functions (IRFs) at three wavelengths: 600 nm, 800 nm, and 1000 nm. The narrow laser pulse allows us to consider these IRFs as almost equal to the SPTR shape, being the response of the detector the main contribution. On the left the bare data are shown while on the right the background noise was subtracted to better point out the exponentially decaying tail.

TABLE I. Performances of the most commonly used PMTs for diffuse optics application and comparison with the SiPM module.

Manufacturer	Name	Area (mm ²)	QE 600 nm (%)	QE 800 nm (%)	SPTR (ps)	DCR (kcps)	Cooled
Hamamatsu Ltd.	R7400U-20	50.2	16.5	7.7	n.d.	<0.4	N
Hamamatsu Ltd.	R5900-20-M4	4 × 81	15.0	7.0	320	n.d.	N
Becker & Hickl	PMC-100	50.2	10.3	4.6	180	0.2-0.5	Y
Becker & Hickl	HPM-100-50	7.1	15.0	13.0	130	0.5-3	N
Picoquant	PMA-192	50.2	18.0	8.0	150	<3	Y
	SiPM module	1	29.9	10.1	100	~100	Y

E. Instrument response function

Figure 6 shows the IRFs obtained for the detector at 6 V of excess bias voltage for three example wavelengths over the characterized spectrum. To obtain the IRF, we directly coupled the laser fiber to the detector, by the means of the focusing optics described in Sec. II. Always keeping a total count rate below the 2.5% of the laser repetition rate, which allows to assume as negligible the pile-up distortion effect, we acquired and summed the photons arrival times for a total integration time of 10 s. The laser temporal width (10 ps FWHM) and the TCSCP board resolution (6 ps FWHM) being well below the module temporal resolution (100 ps FWHM), the the photon's arrival times distribution is essentially dominated by the SiPM response function. The constant background noise has been subtracted to enhance the dynamic range, thus appreciating the whole IRF. As discussed in detail in Ref. 28, the Gaussian peak of the single-photon response, whose temporal resolution is quantified by a FWHM of about 100 ps, is followed by two exponential decaying tails. While the fast tail (decay time constant of ~90 ps) is essentially independent from the wavelength, the slower one (decay time constant of ~3 ns) sets a different limit to the dynamic range depending on the wavelength of excitation. This is probably due to the increase in absorption depth of photons at longer wavelengths. Indeed, while the 600 nm radiation is mainly absorbed within the depleted region of the detector, the 1000 nm one is absorbed more in depth; as a consequence, electron-hole pairs are more often generated within the neutral region of the detector just beyond the depleted active region. In this way, carriers have to slowly diffuse before reaching the high-field region, thus giving rise to the slow tail under discussion.⁴⁴ The distortion preceding the IRF peak at 600 nm is due to a non-ideal behavior of the wavelength selection system of the laser pulse.

IV. CONCLUSIONS

We designed and characterized a fully operative, easy to use, and compact (5 cm × 4 cm × 10 cm) single-photon timing module based on a 1 mm² active area SiPM detector (commercially available from Excelitas Technologies, Canada). To the best of our knowledge, different SiPM modules have been already presented in the literature, but none of them demonstrated the capability to efficiently extract the single-photon timing information, being tailored for photon-number resolving applications. The module features a SPTR of about

100 ps FWHM; it embeds the high biasing voltage generation network and a thermoelectric cooler driver to stabilize the detector temperature, allowing that way both a very short (i.e., about 1 min) warm-up time and a complete insensitivity to possible external thermal perturbations.

This SiPM module can be considered as a fundamental building block for the design of complex systems where picosecond timing information is required together with a wide photon collection area for enhancing the signal harvesting, such as fluorescence decays measurements and time-resolved diffuse optics systems. Referring to Table I that compares some of the most commonly used PMTs for diffuse optics applications, it is worth noting how SiPM modules with such performances can easily replace traditional photocathode-based detectors, being more performing, cheaper, rugged, and reliable, characteristics that reflect into a considerable reduction in the whole system complexity, size and cost.

ACKNOWLEDGMENTS

The research leading to these results has partially received funding from the European Union's Horizon 2020 research and innovation program under Grant Agreement No. 688303 and from Cariplo Foundation under Grant No. 2013-0615.

¹D. V. O'Connor and D. Philips, *Time Correlated Single Photon Counting* (Academic Press, London, 1984).

²W. Becker, A. Bergmann, M. A. Hink, K. König, K. Benndorf, and C. Biskup, "Fluorescence lifetime imaging by time-correlated single-photon counting," *Microsc. Res. Tech.* **63**(1), 58–66 (2004).

³I. Munro, J. McGinty, N. Galletly, J. Requejo-Isidro, P. M. P. Lanigan, D. S. Elson, C. Dunsby, M. A. A. Neil, M. J. Lever, G. W. H. Stamp, and P. M. W. French, "Toward the clinical application of time-domain fluorescence lifetime imaging," *J. Biomed. Opt.* **10**(5), 51403–51409 (2005).

⁴B. Montcel and P. Poulet, "An instrument for small-animal imaging using time-resolved diffuse and fluorescence optical methods," *Nucl. Instrum. Methods Phys. Res., Sect. A* **569**(2), 551–556 (2006).

⁵D. Grosenick, A. Hagen, O. Steinkellner, A. Poellinger, S. Burock, P. M. Schlag, H. Rinneberg, and R. Macdonald, "A multichannel time-domain scanning fluorescence mammograph: Performance assessment and first *in vivo* results," *Rev. Sci. Instrum.* **82**, 2 (2011).

⁶N. A. Hosny, D. A. Lee, and M. M. Knight, "Single photon counting fluorescence lifetime detection of pericellular oxygen concentrations," *J. Biomed. Opt.* **17**(1), 16007–16012 (2012).

⁷A. Yodh and B. Chance, "Spectroscopy and imaging with diffusing light," *Phys. Today* **48**(3), 34–40 (1995).

⁸M. Kacprzak, A. Liebert, P. Sawosz, N. Żolek, and R. Maniewski, "Time-resolved optical imager for assessment of cerebral oxygenation," *J. Biomed. Opt.* **12**(3), 34014–34019 (2007).

⁹H. Wabnitz, M. Moeller, A. Liebert, H. Obrig, J. Steinbrink, and R. Macdonald, in *Oxygen Transport to Tissue XXXI*, edited by E. Takahashi and F. D. Bruley (Springer, Boston, MA, USA, 2010), pp. 143–148.

- ¹⁰Y. Lu, W. Zhang, L. Wu, L. Zhang, and F. Gao, "A time-domain diffuse optical/fluorescent tomography using multi-dimensional TCSPC design," *Proc. SPIE* **8572**, 85721I-1–85721I-7 (2013).
- ¹¹C. Lindner, M. Mora, P. Farzam, M. Squarcia, J. Johansson, U. M. Weigel, I. Halperin, F. A. Hanzu, and T. Durduran, "Diffuse optical characterization of the healthy human thyroid tissue and two pathological case studies," *PLoS One* **11**(1), e0147851 (2016).
- ¹²R. J. Cooper, E. Magee, N. Everdell, S. Magazov, M. Varela, D. Airantzis, A. P. Gibson, and J. C. Hebden, "MONSTIR II: A 32-channel, multispectral, time-resolved optical tomography system for neonatal brain imaging," *Rev. Sci. Instrum.* **85**, 5 (2014).
- ¹³A. Torricelli, D. Contini, A. Dalla Mora, E. Martinenghi, D. Tamborini, F. Villa, A. Tosi, and L. Spinelli, "Recent advances in time-resolved NIR spectroscopy for nondestructive assessment of fruit quality," *Chem. Eng. Trans.* **44**, 43–48 (2015).
- ¹⁴A. Torricelli, D. Contini, A. Pifferi, M. Caffini, R. Re, L. Zucchelli, and L. Spinelli, "Time domain functional NIRS optical imaging for human brain mapping," *Neuroimage* **85**, 28–50 (2014).
- ¹⁵S. Cova, M. Ghioni, A. Lacaita, C. Samori, and F. Zappa, "Avalanche photodiodes and quenching circuits for single-photon detection," *Appl. Opt.* **35**(12), 1956–1976 (1996).
- ¹⁶F. Villa, R. Lussana, D. Bronzi, S. Tisa, A. Tosi, F. Zappa, A. Dalla Mora, D. Contini, D. Durini, S. Weyers, and W. Brockherde, "CMOS imager with 1024 SPADs and TDCS for single-photon timing and 3-D time-of-flight," *IEEE J. Sel. Top. Quantum Electron.* **20**, 6 (2014).
- ¹⁷E. Charbon, "Single-photon imaging in complementary metal oxide semiconductor processes," *Philos. Trans. R. Soc., A* **372**(2012), 20130100 (2014).
- ¹⁸S. Jahromi, J. Jansson, I. Nissinen, J. Nissinen, and J. Kostamovaara, "A single chip laser radar receiver with a 9×9 SPAD detector array and a 10-channel TDC," in *41st European Solid-State Circuits Conference (ESSCIRC)* (IEEE, 2015), pp. 364–367.
- ¹⁹D. Contini, A. Dalla Mora, L. Spinelli, A. Farina, A. Torricelli, R. Cubeddu, F. Martelli, G. Zaccanti, A. Tosi, G. Boso, F. Zappa, and A. Pifferi, "Effects of time-gated detection in diffuse optical imaging at short source-detector separation," *J. Phys. D: Appl. Phys.* **48**(4), 45401 (2015).
- ²⁰A. Puzska, L. Di Sieno, A. Dalla Mora, A. Pifferi, D. Contini, A. Planat-Chrétien, A. Koenig, G. Boso, A. Tosi, L. Hervé, and J.-M. Dinten, "Spatial resolution in depth for time-resolved diffuse optical tomography using short source-detector separations," *Biomed. Opt. Express* **6**(1), 1 (2014).
- ²¹M. Assanelli, A. Ingarciola, I. Rech, A. Gulinatti, and M. Ghioni, "Photon-timing jitter dependence on injection position in single-photon avalanche diodes," *IEEE J. Quantum Electron.* **47**(2), 151–159 (2011).
- ²²S. Cova, A. Lacaita, and G. Ripamonti, "Trapping phenomena in avalanche photodiodes on nanosecond scale," *IEEE Electron Device Lett.* **12**(12), 685–687 (1991).
- ²³F. Villa, D. Bronzi, Y. Zou, C. Scarcella, G. Boso, S. Tisa, A. Tosi, F. Zappa, D. Durini, S. Weyers, U. Paschen, and W. Brockherde, "CMOS SPADs with up to 500 μm diameter and 55% detection efficiency at 420 nm," *J. Mod. Opt.* **61**(2), 102–115 (2014).
- ²⁴B. Dolgoshein, V. Balagura, P. Buzhan, M. Danilov, L. Filatov, E. Garutti, M. Groll, A. Ilyin, V. Kantserov, V. Kaplin, A. Karakash, F. Kayumov, S. Klemin, V. Korbel, H. Meyer, R. Mizuk, V. Morgunov, E. Novikov, P. Pakhlov, E. Popova, V. Rusinov, F. Sefkow, E. Tarkovsky, and I. Tikhomirov, "Status report on silicon photomultiplier development and its applications," *Nucl. Instrum. Methods Phys. Res., Sect. A* **563**(2), 368–376 (2006).
- ²⁵D. Renker, "New trends on photodetectors," *Nucl. Instrum. Methods Phys. Res., Sect. A* **571**(1–2), 1–6 (2007).
- ²⁶P. Buzhan, B. Dolgoshein, L. Filatov, A. Ilyin, V. Kantserov, V. Kaplin, A. Karakash, F. Kayumov, S. Klemin, E. Popova, and S. Smirnov, "Silicon photomultiplier and its possible applications," *Nucl. Instrum. Methods Phys. Res., Sect. A* **504**(1–3), 48–52 (2003).
- ²⁷D. R. Schaart, H. T. van Dam, S. Seifert, R. Vinke, P. Dendooven, H. Löhner, and F. J. Beekman, "A novel, SiPM-array-based, monolithic scintillator detector for PET," *Phys. Med. Biol.* **54**(11), 3501–3512 (2009).
- ²⁸E. Martinenghi, A. Dalla Mora, D. Contini, A. Farina, F. Villa, A. Torricelli, and A. Pifferi, "Spectrally resolved single-photon timing of silicon photomultipliers for time-domain diffuse spectroscopy," *IEEE Photonics J.* **7**(4), 1–12 (2015).
- ²⁹C. Zhang, L. Zhang, R. Yang, K. Liang, and D. Han, "Time-correlated Raman and fluorescence spectroscopy based on a silicon photomultiplier and time-correlated single photon counting technique," *Appl. Spectrosc.* **67**(2), 136–140 (2013).
- ³⁰A. Dalla Mora, D. Contini, S. Arridge, F. Martelli, A. Tosi, G. Boso, A. Farina, T. Durduran, E. Martinenghi, A. Torricelli, and A. Pifferi, "Towards next-generation time-domain diffuse optics for extreme depth penetration and sensitivity," *Biomed. Opt. Express* **6**(5), 1749 (2015).
- ³¹A. Dalla Mora, E. Martinenghi, D. Contini, A. Tosi, G. Boso, T. Durduran, S. Arridge, F. Martelli, A. Farina, A. Torricelli, and A. Pifferi, "Fast silicon photomultiplier improves signal harvesting and reduces complexity in time-domain diffuse optics," *Opt. Express* **23**(11), 13937 (2015).
- ³²S. Fujisaka, T. Ozaki, T. Suzuki, T. Kamada, K. Kitazawa, M. Nishizawa, A. Takahashi, and S. Suzuki, "A clinical tissue oximeter using NIR time-resolved spectroscopy," in *Proceedings of the 43rd Annual Meeting of the International Society on Oxygen Transport to Tissue (ISOTT)*, 2016.
- ³³I. Bargigia, A. Tosi, A. B. Shehata, A. Della Frera, A. Farina, A. Bassi, P. Taroni, A. Dalla Mora, F. Zappa, R. Cubeddu, and A. Pifferi, "Time-resolved diffuse optical spectroscopy up to 1700 nm by means of a time-gated InGaAs/InP single-photon avalanche diode," *Appl. Spectrosc.* **66**(8), 944–950 (2012).
- ³⁴S. M. Sze and K. N. Kwok, *Physics of Semiconductor Devices* (Wiley, New York, 1981).
- ³⁵M. Mazzillo, G. Condorelli, D. Sanfilippo, G. Valvo, B. Carbone, A. Piana, G. Fallica, A. Ronzhin, M. Demartean, S. Los, and E. Ramberg, "Timing performances of large area silicon photomultipliers fabricated at STMicroelectronics," *IEEE Trans. Nucl. Sci.* **57**(4), 2273–2279 (2010).
- ³⁶V. Puill, C. Bazin, D. Breton, L. Burmistrov, V. Chaumat, N. Dinu, J. Maalmi, J. F. Vagnucci, and A. Stocchi, "Single photoelectron timing resolution of SiPM as a function of the bias voltage, the wavelength and the temperature," *Nucl. Instrum. Methods Phys. Res., Sect. A* **695**, 354–358 (2012).
- ³⁷F. Acerbi, A. Ferri, A. Gola, M. Cazzanelli, L. Pavesi, S. Member, N. Zorzi, and C. Piemonte, "Characterization of single-photon time resolution: From single SPAD to silicon photomultiplier," *IEEE Trans. Nucl. Sci.* **61**(5), 2678–2686 (2014).
- ³⁸W. Becker, *The Bh TCSPC Handbook*, 6th ed. (Becker & Hickl, 2014).
- ³⁹F. Villa, Y. Zou, A. Dalla Mora, and A. Tosi, "Spice electrical models and simulations of silicon photomultipliers," *IEEE Trans. Nucl. Sci.* **62**(5), 1950–1960 (2015).
- ⁴⁰E. Sciacca, A. C. Giudice, D. Sanfilippo, F. Zappa, S. Lombardo, R. Consentino, C. Di Franco, M. Ghioni, G. Fallica, G. Bonanno, S. Cova, and E. Rimini, "Silicon planar technology for single-photon optical detectors," *IEEE Trans. Electron Devices* **50**(4), 918–925 (2003).
- ⁴¹A. Tosi, A. Dalla Mora, F. Zappa, and S. Member, "All-silicon 1.55 μm high-resolution photon counting and timing," *IEEE Photonics Technol. Lett.* **20**(23), 1956–1958 (2008).
- ⁴²C30742–11 series datasheet, available at www.excelitas.com.
- ⁴³SPCM-AQRH Datasheet, available at www.excelitas.com.
- ⁴⁴M. Ghioni, A. Gulinatti, I. Rech, F. Zappa, and S. Cova, "Progress in silicon single-photon avalanche diodes," *IEEE J. Sel. Top. Quantum Electron.* **13**(4), 852–862 (2007).